

Kiho Jung · Akihisa Kitamori · Kohei Komatsu

Development of a joint system using a compressed wooden fastener I: evaluation of pull-out and rotation performance for a column–sill joint

Received: September 17, 2008 / Accepted: January 14, 2009 / Published online: May 14, 2009

Abstract Compressed wooden plates and dowels were used to connect members in post-and-beam structures as a substitute for a steel fastener. In order to take advantage of the characteristic properties of compressed wood and to achieve optimum joint performance, two compressed wooden plates were used in each joint to give multiple shear planes for each compressed wooden dowel. Consequently, this type of joint showed very good properties in pull-out and moment-rotation performance, and its engineering design could be further optimized. This joint is expected to be introduced to many kinds of structural systems, including long-span frame structures made of domestic timber found in Japanese residential houses.

Key words Post-and-beam structure · Compressed wood · Pull-out · Moment rotation · Long-span frame

Introduction

Compressed wood (CW) was developed for effective utilization of low-density material such as Japanese cedar, which is relatively abundant in Japan, and has been gradually introduced as a joint material in Japanese post-and-beam structures.^{1,2} CW may be suitable for use as a fastener in locations where severe compression or shear stress concentration occurs, by virtue of its high material properties and because it can be produced with high densities. Moreover, as reported previously, its characteristic good performance in double shear perpendicular to the grain gives it high potential as a shear dowel.³

Therefore, a CW plate-and-dowel-type fastener was suggested to achieve a perfectly natural wood-to-wood joint system against the background of developing an eco-friendly

post-and-beam structure with high performance. This research evaluated pull-out and rotation performance for a CW plate-and-dowel-insertion type of column–sill joint. In detail, a mechanical model for this type of joint was proposed and compared with experimental results with the aim of developing optimum design. The ultimate goal of this research was to use a metal-free, eco-friendly timber joint system in Japanese residential houses.

Theory

In the design concept, in order to take advantage of the characteristic properties of CW, two insertion-type CW plates were proposed.⁴ This is because, first, making a CW thin plate is relatively easy, and, second, it gives multiple shear layers for each compressed dowel as shown in Fig. 1. Moreover, in this type of joint system the dowel's position of sill area can be shifted farther toward the bottom side than in a conventional mortise and tenon joint, because the shear strength of the CW plate in the radial (L_R) plane is almost three times that of normal Japanese cedar wood. Consequently, this will give good performance not only for pull-out but also for rotation. In addition, brittle failure on the sill area seems unlikely, because the CW dowel has sufficient ductility.

Pull-out model

Two types of springs for pull-out of the CW column–sill joint can be assumed, which represent the shear resistance of the dowel on the column given to CW plates, and that on the CW plate given to the sill. Hence, stiffness of the joint as shown in Fig. 2 can be expressed by Eq. 1.

$$K_{\text{Joint}} = \frac{K_{\text{Column}} \cdot K_{\text{Sill}}}{K_{\text{Column}} + K_{\text{Sill}}} \quad (1)$$

$$K_{\text{Column}} = n_C \cdot n_P \cdot K_{b0p0d0}, \quad K_{\text{Sill}} = n_S \cdot n_P \cdot K_{b90p0d0},$$

K. Jung (✉) · A. Kitamori · K. Komatsu
Research Institute for Sustainable Humanosphere, Kyoto University,
Gokasyou, Uji, Kyoto 611-0011, Japan
Tel. +81-774-38-3670; Fax +81-774-38-3678
e-mail: jungkiho@rish.kyoto-u.ac.jp

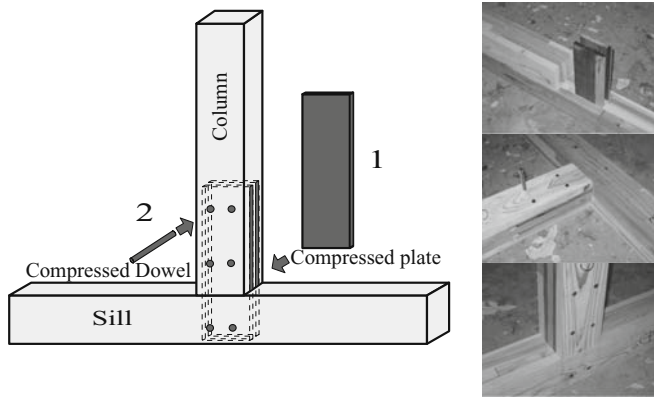
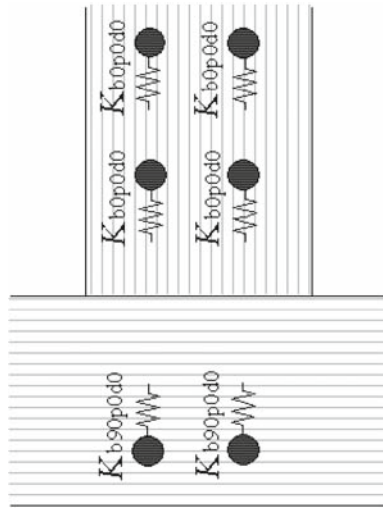


Fig. 1. Design concept for column-sill joint

Fig. 2. Spring model



where n_C and n_S are the number of dowels, n_p is the number of plates, and K_{b0p0d0} and $K_{b90p0d0}$ represent the stiffness of dowel in each direction.

Shear deformation and yielding will mainly occur on the sill area, because dowel shear strength parallel to the grain direction of the column and the CW plate is stronger than that perpendicular to the grain direction of the sill when at least the same number of dowels are inserted on the column area. Thus, the yield model was considered only on the sill area. This was calculated by modified european yield theory (EYT) expressed by Eqs. 2 and 3 based on our previous report.^{1,2}

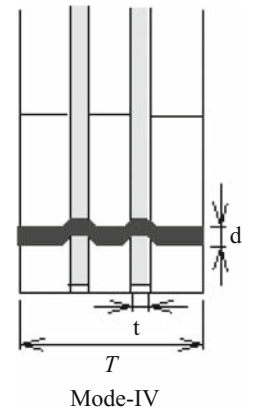
$$P_y = n_p \cdot C \cdot F'_m \cdot d \cdot t \quad (2)$$

$$C = \frac{2d}{t} \kappa \quad (3)$$

where F'_m is $\min[F_m, F_d]$, $\kappa = S_d/F'_m$, F_m is the embedding strength of plate, F_d is the embedding strength of dowel, and S_d is the shear strength of dowel perpendicular to the grain.

A CW dowel with its annual ring radial to the loading direction has only yield mode VI as shown in Fig. 3, in which yield occurs not by bending but by shear on the dowel.

Fig. 3. Yield mode



Thus, the yielding strength of the CW-dowel type of joint, which has multiple shears, can be easily estimated.^{1,2}

Rotational model

Stiffness

The CW-dowel type of joint has very complex behavior in rotational performance, because the CW plate, which is connected between the column and the sill area, is fixed by CW dowels in each area. When a rotational moment is applied to the CW column-sill joint, resistance and deformation can be thought of as being divided into two areas, which are the column area and the sill area. In both parts, relative deformation against CW plate is considered. Furthermore, horizontal and vertical directions are considered separately.

Whole deformation against the rotational moment depends on correlative balance between these two areas. Two factors can be expected: shearing resistance by the dowels, and embedding resistance between each member on the joint. Rotation center, stiffness, and deformation angle on each area will be changed by balance between these resistance factors. In order to simplify the mechanical behavior model, we divided each resistance factor on each area for the horizontal (Fig. 4) and vertical (Fig. 5) directions on rotational moment. First, the relationship between moment and deformation on each area for the whole joint is shown in Eq. 4

$$M_J = \left(\frac{H}{H-h} \right) M_C = M_S, \quad \theta_J = \theta_C + \theta_S \quad (4)$$

where M_J , M_C , and M_S are rotational moments for whole joint, column area, and sill area, and θ_J , θ_C , and θ_S are deformational angles for whole joint, column area, and sill area. Each moment for the horizontal and vertical directions is shown in Eq. 5

$$M_C = M_{CH} + M_{CV}, \quad M_S = M_{SH} + M_{SV} \quad (5)$$

where, M_{CH} and M_{CV} are rotational moments for horizontal and vertical direction on the column area, and M_{SH} and M_{SV} are rotational moments for horizontal and vertical direction on the sill area.

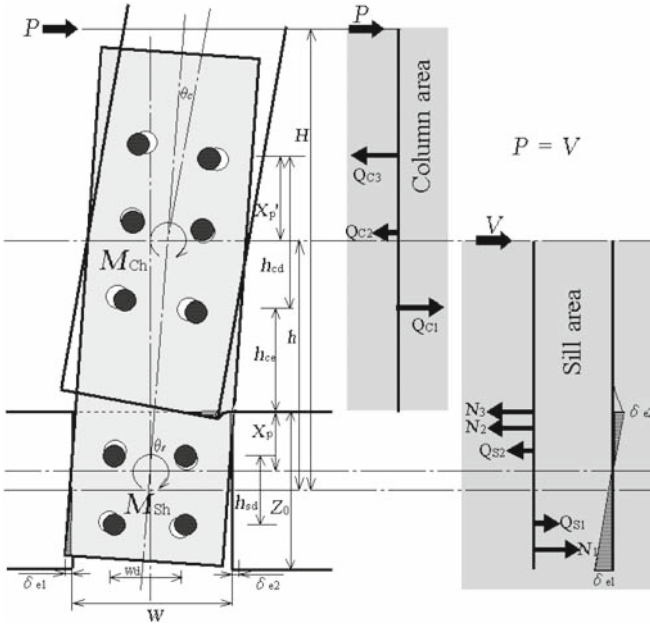


Fig. 4. Horizontal direction. X_p and X'_p are distances to each center on two rotational areas. Deformation model and assumption for equilibrium of force on Horizontal direction

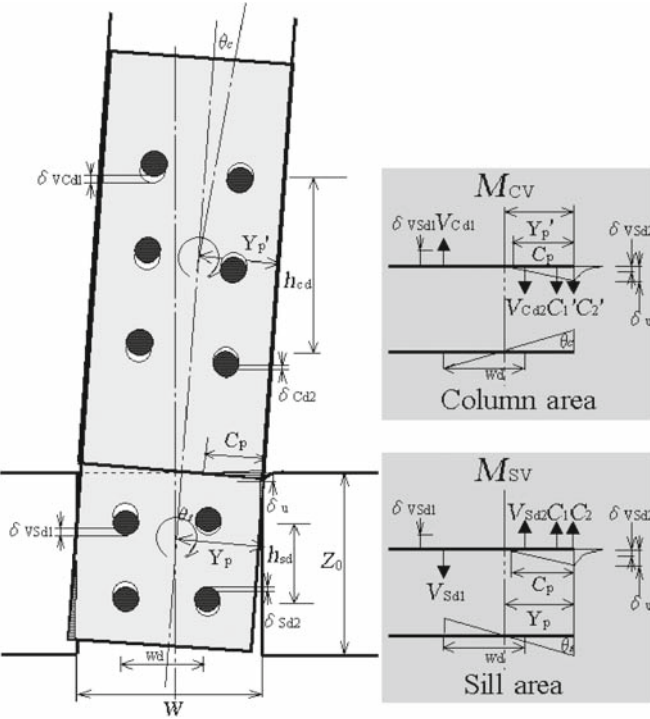


Fig. 5. Vertical direction. Y_p and Y'_p are distances to each center on two rotational areas. Deformation model and assumption for equilibrium of force on Vertical direction

Horizontal direction: column area

Moment resistance for the horizontal direction on the column area is caused by shear resistance (Q_{C1} , Q_{C2} , and Q_{C3}) by each CW dowel. These shear resistances can be expressed by Eq. 6

$$\begin{aligned} Q_{C1} &= A'_1(h_{cd} - X'_p)\theta_C, & Q_{C2} &= A'_2\left(X'_p - \frac{h_{cd}}{2}\right)\theta_C, \\ Q_{C3} &= A'_1X'_p\theta_C \end{aligned} \quad (6)$$

where $A'_1 = n_{HCd1}n_pK_{b90p90d90}$, $A'_2 = n_{HCd2}n_pK_{b90p90d90}$, n_{HCd1} and n_{HCd2} are numbers of dowel on each position [$n_{HCd1} = 2$, $n_{HCd2} = 0$ (total number on the column is 4), $n_{HCd1} = 2$, $n_{HCd2} = 2$ (total number on the column is 6)], and $K_{b90p90d90}$ is stiffness of dowel for each direction.

Equilibrium of horizontal shear forces and that of moment at the center of the sill give Eq. 7

$$\begin{aligned} P + Q_{C1} &= Q_{C2} + Q_{C3}, \\ PH + bQ_{C1} - \left(b + \frac{h_{cd}}{2}\right)Q_{C2} - (b + h_{cd})Q_{C3} &= 0 \end{aligned} \quad (7)$$

where $b = h_{ce} + \frac{Z_0}{2}$. Substituting Eq. 6 into Eq. 7, Eq. 8 for rotational center (X'_p) on the column area can be obtained.

$$X'_p = \frac{2h_{cd}(2A'_1 + A'_2)(H - b) - h_{cd}^2A'_2}{4(2A'_1 + A'_2)(H - b) - 2h_{cd}(A'_2 + 2A'_1)} \quad (8)$$

Moment (M_{CH}) and stiffness (R_{CH}) for horizontal direction on column area are expressed by Eqs. 9 and 10.

$$M_{CH} = (h_{cd} - X'_p)Q_{C1} + \left(X'_p - \frac{h_{cd}}{2}\right)Q_{C2} + X'_pQ_{C3} \quad (9)$$

$$R_{CH} = A'_1(h_{cd} - X'_p)^2 + A'_2\left(X'_p - \frac{h_{cd}}{2}\right)^2 + A'_1X'^2_p \quad (10)$$

Horizontal direction: sill area

In the horizontal direction, we can presume first that load (P) is delivered from the column to the CW plate by shearing of dowel, and, second, that it is redelivered into the sill through the CW plate. Assuming this load transmission mechanism, we took the same approach as in the case of the column for estimating horizontal moment on the sill. Moment resistance for the sill area consists of shearing resistance by the dowels (Q_{S1} and Q_{S2}) and embedding resistance (N_1 , N_2 , and N_3) between the CW plates and the sill. Here, N_3 is resisting force by the additional length effect on the CW plate, which depends on Inayama's theory.^{5,6} These can be expressed as Eqs. 11

$$\begin{aligned} Q_{S1} &= A_1(\alpha_1 - X_p)\theta_S, & Q_{S2} &= A_2|X_p - \alpha_2|\theta_S, \\ (X_p \geq \alpha_2) \text{ or } (X_p \leq \alpha_2) & & & \\ N_1 &= \frac{1}{2}\alpha_3(Z_0 - X_p)^2\theta_S, & N_2 &= \frac{1}{2}\alpha_3X_p^2\theta_S, & N_3 &= \frac{2}{3}\alpha_3WX_p\theta_S \end{aligned} \quad (11)$$

where $A_1 = n_{HSd1} \cdot n_p \cdot K_{b90p90d90}$, $A_2 = n_{HSd2} \cdot n_p \cdot K_{b90p90d90}$, $\alpha_1 = \frac{Z_0 + h_{sd}}{2}$, $\alpha_2 = \frac{Z_0 - h_{sd}}{2}$, $\alpha_3 = n_p \cdot t \cdot K_{(Plate90+Sill0)}$, n_{HSd} is the number of dowels on each position, and $K_{b90p90d90}$ is the stiffness of dowel for each direction.

Combination of embedding stiffness of CW plate and sill can be calculated by Eq. 12⁷

$$K_{(Plate90+Sill0)} = \frac{K_{(Plate90)} \cdot K_{(Sill0)}}{K_{(Plate90)} + K_{(Sill0)}} \quad (12)$$

where $K_{(\text{Plate90})} = \frac{E_{(\text{CW90})}}{W}$, $K_{(\text{Sill0})} = \frac{E_{(\text{cedar0})}}{31.6 + 10.9 \cdot t}$. We assume that reaction force V of applied force P acts on the column-side rotational center X'_p . Here, rotational center (X_p) on sill area might be changed due to balance of embedding and shearing resistance; therefore, we considered both cases of $X_p \geq \alpha_2$ and $X_p \leq \alpha_2$.

Equilibrium of horizontal shear forces at the sill area gives Eq. 13

$$\begin{aligned} V + Q_{S1} + N_1 &= Q_{S2} + N_2 + N_3 (X_p \geq \alpha_2), \\ V + Q_{S1} + Q_{S2} + N_1 &= N_2 + N_3 (X_p \leq \alpha_2), \quad X_p = \frac{\delta_{e2}}{\theta_S} \end{aligned} \quad (13)$$

Equilibrium of moments gives Eqs. 14

$$\begin{aligned} \frac{1}{3}(Z_0 - X_p)N_1 + \frac{1}{2}(Z_0 - h_{sd})Q_{S1} - \frac{1}{2}(Z_0 + h_{sd})Q_{S2} - \\ \left(Z_0 - \frac{1}{3}X_p\right)N_2 - Z_0N_3 + \alpha_4V = 0 \quad (X_p \geq \alpha_2), \end{aligned} \quad (14)$$

$$\begin{aligned} \frac{1}{3}(Z_0 - X_p)N_1 + \frac{1}{2}(Z_0 - h_{sd})Q_{S1} + \frac{1}{2}(Z_0 + h_{sd})Q_{S2} - \\ \left(Z_0 - \frac{1}{3}X_p\right)N_2 - Z_0N_3 + \alpha_4V = 0 \quad (X_p \leq \alpha_2) \end{aligned}$$

where $\alpha_4 = Z_0 + h_{be} + h_{bd} - X'_p$. By substituting Eqs. 11–13 into Eqs. 14, Eq 15 for rotational center (X_p) on the sill area can be obtained.

$$X_p = \frac{3A_1\alpha_1(Z_0 - h_{sd} - 2\alpha_4) + 3A_2\alpha_2(Z_0 + h_{sd} - 2\alpha_4) + \alpha_3Z_0^2(Z_0 - 3\alpha_4)}{3A_1(Z_0 - h_{sd} - 2\alpha_4) + 3A_2(Z_0 + h_{sd} - 2\alpha_4) + 4\alpha_3W(Z_0 - \alpha_4) + 3\alpha_3Z_0(Z_0 - 2\alpha_4)} \quad (15)$$

Moment (M_{SH}) and stiffness (R_{SH}) for horizontal direction on the sill area can be expressed as Eqs. 16 and 17.

$$\begin{aligned} M_{SH} &= (\alpha_1 - X_p)Q_{S1} + |X_p - \alpha_2|Q_{S2} \\ &+ \frac{2}{3}\alpha_3(Z_0 - X_p)N_1 + \frac{2}{3}\alpha_3X_pN_2 + X_pN_3 \end{aligned} \quad (16)$$

$$\begin{aligned} R_{SH} &= A_1(\alpha_1 - X_p)^2 + A_2(X_p - \alpha_2)^2 + \frac{1}{3}\alpha_3(Z_0 - X_p)^3 + \\ &\frac{1}{3}\alpha_3X_p^3 + \frac{2}{3}\alpha_3WX_p^2 \end{aligned} \quad (17)$$

Vertical direction

For the vertical factor, the same analytical approach as taken in the case of the horizontal direction was used. Firstly, vertical shear resisting forces (V_{CD1} and V_{CD2}) and embedding resisting forces (C'_1 and C'_2) on the column area are expressed by Eqs. 18. C'_2 is also resistance by the additional length effect on the sill area, which depends on Inayama's theory.^{5,6} Embedding resistance between column and sill was assumed to act separately in each area.

$$\begin{aligned} V_{CD1} &= B'(\beta'_1 - Y'_p)\theta_C, \quad V_{CD2} = B'(Y'_p - \beta'_2)\theta_C, \\ C'_1 &= \frac{1}{2}\beta'_3Y_p'^2\theta_S, \quad C'_2 = \frac{2}{3}\beta'_3Z_0Y_p'\theta_C \end{aligned} \quad (18)$$

where $B' = n_{VCD} \cdot n_p \cdot K_{b0p0d0}$, $\beta'_1 = \frac{W + W_d}{2}$, $\beta'_2 = \frac{W - W_d}{2}$, $\beta'_3 = \frac{(T - n_p \cdot t)E_{90}}{Z_0}$, n_{VCD} is the number of dowels on each position, and K_{b0p0d0} is stiffness of dowel for each direction.

Shear-resisting forces on the sill area can be expressed by Eqs. 19

$$\begin{aligned} V_{Sd1} &= B(\beta_1 - Y_p)\theta_S, \quad V_{Sd2} = B(Y_p - \beta_2)\theta_S, \\ C_1 &= \frac{1}{2}\beta_3Y_p^2\theta_S, \quad C_2 = \frac{2}{3}\beta_3Z_0Y_p\theta_S \end{aligned} \quad (19)$$

where $B = n_{Vsd} \cdot n_p \cdot K_{b0p0d0}$, $\beta_1 = \frac{W + W_d}{2}$, $\beta_2 = \frac{W - W_d}{2}$, $\beta_3 = \frac{(T - n_p \cdot t)E_{90}}{Z_0}$, n_{Sd1} and n_{Sd2} are numbers of dowel at each position, and K_{b0p0d0} is the stiffness of dowel for each direction.

Equilibrium of shear forces gives Eqs. 20.

$$V_{CD1} = V_{CD2} + C'_1 + C'_2, \quad V_{Sd1} = V_{Sd2} + C_1 + C_2 \quad (20)$$

Substituting Eqs. 18 and 19 into Eqs. 20, we could obtain Eq. 21 for each rotational center (Y'_p and Y_p)

$$\begin{aligned} Y'_p &= \sqrt{\frac{2B'(\beta'_1 + \beta'_2) + \left(\frac{2\beta'_3Z_0 + 6B'}{3\beta'_3}\right)^2}{\beta'_3}} - \frac{2\beta'_3Z_0 + 6B'}{3\beta'_3}, \\ Y_p &= \sqrt{\frac{2B(\beta_1 + \beta_2) + \left(\frac{2\beta_3Z_0 + 6B}{3\beta_3}\right)^2}{\beta_3}} - \frac{2\beta_3Z_0 + 6B}{3\beta_3} \end{aligned} \quad (21)$$

Rotational center (C_p) between the column and sill can be calculated by Eq. 22 if it is assumed to be located on the shortest line between two rotational centers (Y'_p and Y_p).

$$C_p = \left| Y_p + \frac{X'_p(Y_p - Y'_p)}{(X'_p + X_p)} \right| \quad (22)$$

Moment (M_{CV}) and stiffness (R_{CV}) for vertical direction on the column area can be expressed as Eqs. 23 and 24

$$M_{CV} = (\beta'_1 - Y'_p)V_{CD1} + (Y'_p - \beta'_2)V_{CD2} + \frac{2}{3}C_pC'_1 + C_pC'_2 \quad (23)$$

$$R_{CV} = B'(\beta'_1 - Y'_p)^2 + B'(Y'_p - \beta'_2)^2 + \frac{1}{3}\beta'_3C_p^3 + \frac{2}{3}\beta'_3Z_0C_p^2 \quad (24)$$

Moment derived from friction (Γ) between the CW plate and the sill by rotational deformation of the CW plate can be calculated by Eq. 25 as substituted by Eq. 11. Here, although the factor of friction should be contained in equilibrium for the vertical direction in Eq. 20, the rotational center (Y_p) was induced without considering friction in order to avoid complexity. Consequently, moment derived from friction (Γ) was added to moment (M_{SV}) and stiffness (R_{SV}) for vertical direction on the sill area.

$$\begin{aligned} \Gamma &= \frac{1}{2}(N_1 + N_2 + N_3)\mu W \\ &= \frac{1}{2} \left(\frac{1}{2}\alpha_3(Z_0 - X_p)^2\theta_S + \frac{1}{2}\alpha_3X_p^2\theta_S + \frac{2}{3}\alpha_3WX_p\theta_S \right) \mu W \end{aligned} \quad (25)$$

where μ is the coefficient of friction between the CW plate and the sill; we used 0.35 as coefficient of friction.

Moment (M_{SV}) and stiffness (R_{SV}) for vertical direction on the sill area can be expressed as Eqs. 26 and 27.

$$M_{SV} = (\beta_1 - Y_P)V_{Sd1} + (Y_P - \beta_2)V_{Sd2} + \frac{2}{3}C_P C_1 + C_P C_2 + \Gamma \quad (26)$$

$$R_{SV} = B(\beta_1 - Y_P)^2 + B(Y_P - \beta_2)^2 + \frac{1}{3}\beta_3 C_P^3 + \frac{2}{3}\beta_3 Z_0 C_P^2 + \frac{1}{2}\left(\frac{1}{2}\alpha_3(Z_0 - X_P)^2 + \frac{1}{2}\alpha_3 X_P^2 + \frac{2}{3}\alpha_3 W X_P\right)\mu W \quad (27)$$

Yielding moment

In analyzing the yielding moment, we consider the operation of yielding of the shear dowel on the column area, and yielding of the shear dowel and embedding on the sill area.

Column area

If we suppose that no split occurs on the column and CW plate but only yielding by shear of the dowel, the yielding moment for the column area can be calculated by the shearing yield strength of the dowel with rotational center (X'_P , Y'_P). Here, we assume that this rotational center (X'_P , Y'_P) does not change even after yielding. The relationship between moment and stiffness for column area can be expressed as Eq. 28 as substituted by Eqs. 10 and 24.

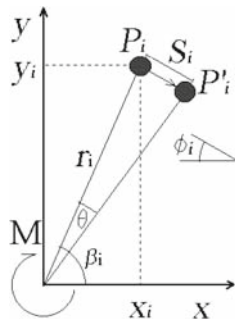
$$M_C = M_{CH} + M_{CV} = (R_{CH} + R_{CV})\theta_C \quad (28)$$

The slip load that one dowel receives at i position by moment (M) as shown in Fig. 6 can be calculated by Eq. 29

$$P_{Si} = K_{\phi i} \cdot r_i \cdot \theta_C \quad (29)$$

Here, K_{ϕ} (slip modulus) for angle ϕ is presumed calculable by integrating K_{b0p0d0} and $K_{b0p0d90}$ for 0° and 90° , respectively, by definition of Hankinson theory. x_i and y_i are coordinates for each dowel at column surface (x_i , horizontal coordinate; y_i , vertical coordinate), and r_i is defined as the distance from rotation center (X'_P , Y'_P) to the position of each dowel.

Fig. 6. Shearing of dowel at position i for moment



$$\phi_i = \frac{\pi}{2} - \beta_i = \frac{\pi}{2} - \tan^{-1}\left(\frac{x_i}{y_i}\right),$$

$$K_{\phi i} = n_P \frac{K_{b0p0d0i} \cdot K_{b90p90d90i}}{K_{b0p0d0i} \sin^2 \phi_i + K_{b90p90d90i} \cos^2 \phi_i},$$

$$r_i = \sqrt{(x_i)^2 + (y_i)^2}$$

Substituting Eq. 28 into Eq. 29, Eq. 30 can be obtained.

$$P_{Si} = K_{\phi i} \cdot r_i \cdot \frac{M_C}{(R_{CH} + R_{CV})} \quad (30)$$

The joint was presumed to reach yielding point when this P_{Si} became equal to P_{Wi} . At this point, yielding moment can be obtained by Eq. 31

$$M_{y-d} = \min\left[\frac{P_{Wi} \cdot (R_{CH} + R_{CV})}{K_{\phi i} \cdot r_i}\right] \quad (31)$$

where i represents each dowel and M_y is determined by taking minimum value among all dowels. Here, yielding strength (P_{Wi}) of each dowel for angle ϕ can be calculated by Hankinson theory with $P_{yb0p0d0}$ and $P_{y0p0d90}$ for angles of 0 and 90 degrees.

$$P_{Wi} = n_P \frac{P_{yb0p0d0i} \cdot P_{y0p0d90i}}{P_{yb0p0d0i} \sin^2 \phi_i + P_{y0p0d90i} \cos^2 \phi_i}$$

Sill area

Yielding by shearing of dowel and embedding between the CW plate and the sill part should be taken into account for pursuing the yielding moment (M_{y-s}) on the sill area, in view of the fact that these two factors play mutual, important roles on rotational performance. The lowest value between yielding moments by shearing of dowel, embedding of compressed plate, and embedding of the sill is defined as the yielding moment of the sill area, as in Eq. 32.

$$M_{y-s} = \min[M_{y-d}, M_{y-cw}, M_{y-sill}] \quad (32)$$

The same equation as that for the column was applied for estimating the yielding moment by shearing of dowel on the sill area. The only difference is the shearing direction of dowel for the main members. The yielding moment by shearing of dowel at the sill area can be calculated by Eq. 31 with those factors in Eq. 33 and stiffness of sill part.

$$K_{\phi i} = n_P \frac{K_{b90p0d0i} \cdot K_{b0p90d90i}}{K_{b90p0d0i} \sin^2 \phi_i + K_{b0p90d90i} \cos^2 \phi_i},$$

$$P_{yi} = n_P \frac{P_{yb90p0d0i} \cdot P_{yb0p90d90i}}{P_{yb90p0d0i} \sin^2 \phi_i + P_{yb0p90d90i} \cos^2 \phi_i} \quad (33)$$

Yielding angle and moment by embedding of the CW plate can be calculated by Eq. 34 using Inayama's theory.⁶

$$M_{y-cw} = R_{\theta} \cdot \theta_{y-cw}, \quad \theta_{y-cw} = \frac{WF_m(CW90)}{X_P E_{CW90} \sqrt{C_x C_{xm} C_{ym}}},$$

$$C_x = 1 + \frac{2W}{3X_P} \left(2 - e^{-\frac{3x_1}{2W}}\right), \quad C_{xm} = 1 + \frac{4W}{3X_P},$$

$$C_{ym} = 1 + \frac{4W}{3nnpt} \quad (34)$$

Because CW plate has high embedding strength, yielding of the sill is possible as shown in Fig. 7. The embedding stress distribution of the sill is assumed as triangle, although that of the CW plate is assumed as triangle and the effect by additional length separately. Reaction force (C) of the sill is same with embedding resistance ($N_1 + N_2$) of CW plate. It is supposed that yield occurs when maximum stress at the edge of the sill reaches the yielding strength (F_C) of the sill.

Thus, Eqs. 35 from Eqs. 11 can be formed when yielding of the sill occurs

$$C_{\text{Sill}} = N_2 + N_3, \quad C = \frac{1}{2} n_p \cdot t \cdot F_C \cdot X_p \quad (35)$$

Substituting Eq. 11 into Eq. 35, yielding angle and moment by embedding of the sill can be calculated by Eq. 36

$$M_{y-\text{sill}} = (R_{\text{SH}} + R_{\text{SV}}) \cdot \theta_{y-\text{sill}}, \quad \theta_{y-\text{sill}} = \frac{n_p t X_p F_C \theta_s}{2(N_2 + N_3)} \quad (36)$$

where $F_C = 60.68 \cdot \rho$ and ρ is density of wood.

Experimental

Material

E60-F225 grade Japanese cedar glulam was used for column and sill (120×120 mm). CW plate and dowel material was compressed in the radial direction at a temperature of 130°C for 30 min. No fixation treatment, such as steaming, chemical agent, or resin, was applied. Apparent density was

increased from 0.33 to 0.88 g/cm^3 on the CW plate and to 1.1 g/cm^3 on CW dowel by applying compression ratios of 62% and 70%, respectively. In this case, the density of CW plate was relatively low to avoid damaging the base member by swelling stress. In preparing material for making CW, all boards selected for compression had flat annual growth rings and were free of knots, splits, and pith. Initial moisture content was approximately 12% prior to the compression process. For fabrication of the dowels, the wood pieces had initial dimensions of 15×15 mm and were then processed into round shapes with a final diameter of 12 mm. The process of making the compressed wooden plates was almost the same as that for the dowel, differing only by the compression ratio. The plate size was $120 \times 360 \times 14$ mm for the column-to-sill joint.

Pull-out test

A pull-out test was performed to evaluate the efficiency and failure mechanism of the column-sill joint. Figure 8 and Table 1 present the details of the column-sill joint pull-out tests.

Figure 9 shows the experimental apparatus for the pull-out test. The sill member was fixed by bolts (diameter 16 mm) with a 1000-mm span. The loaded end of the column was fixed to a steel jig with ten lag screws (diameter 8 mm). This steel jig was connected to a load cell and a hydraulic actuator. Pull-out load was applied to the specimen by this actuator via a computer-controlled system. Relative displacements between column and sill were measured by means of two displacement transducers (CDP-50) attached to both faces of the column, and those between the plate and column and between the plate and the sill were also measured by using four displacement transducers (CDP-25).

Fig. 7. Embedding of sill

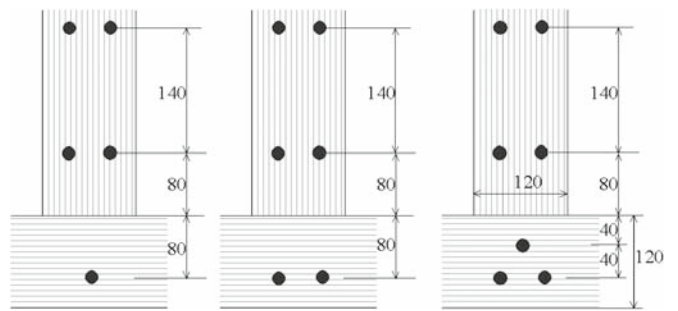
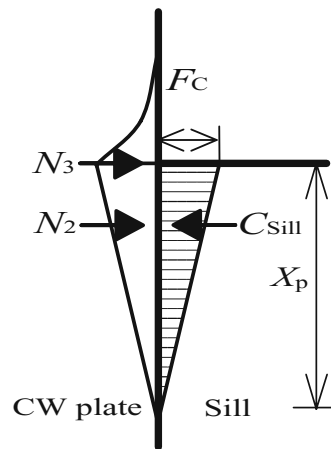


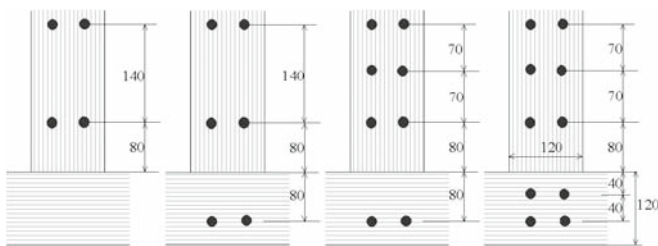
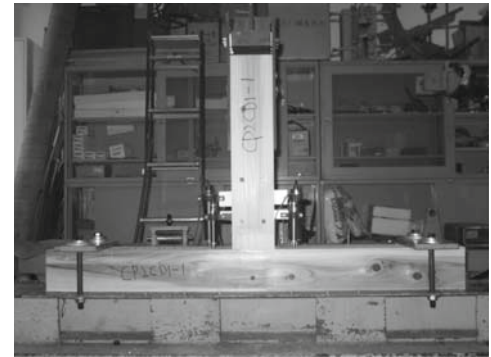
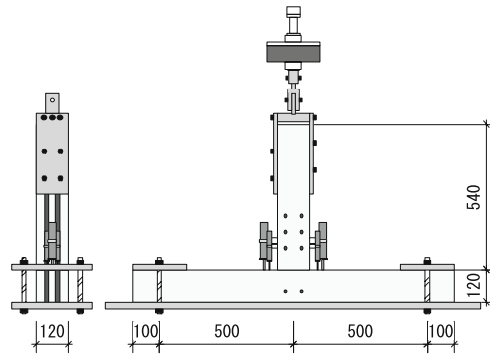
Fig. 8. Parameters of column-sill joint for pull-out test

Table 1. Parameters of column-sill joints for pull-out tests

Specimen	Dimensions (mm)				Number of dowels		No.
	Column	Sill	Plate	Dowel diameter (mm)	Column	Sill	
PCP2C4S1	$120 \times 120 \times 560$	$120 \times 120 \times 1200$	$120 \times 360 \times 15$	12	4	1	3
PCP2C4S2				12	4	2	3
PCP2C4S3				12	4	3	3

Table 2. Parameters of column–sill joints for rotation tests

Specimen	Dimensions (mm)				Number of dowels		No.
	Column	Sill	Plate	Dowel diameter (mm)	Column	Sill	
RCP2C4S0	120 × 120 × 560	120 × 120 × 1200	120 × 360 × 15	12	4	0	3
RCP2C4S2				12	4	2	3
RCP2C6S2				12	6	2	3
RCP2C6S4				12	6	4	3

Fig. 9. Apparatus for pull-out test of column–sill joint**Fig. 10.** Parameters of column–sill joint for rotation test

Rotation test

A rotation test was performed to evaluate the performance of the column–sill joint under rotational moment (M). Figure 10 and Table 2 shows the parameters of the column–sill joint for the rotation test.

Figure 11 shows the experimental apparatus for the rotation test of the column–sill joint. The rotation moment was applied by a quadratic-link steel frame. Each member of the steel frame was 1000 mm in length, and they were connected by pins. A load was applied by a hydraulic actuator. As shown in Fig. 8, each specimen was set at center of the frame and jointed with steel pins (diameter 22 mm). The loading schedule was 1/300, 1/200, 1/150, 1/100, 1/75, 1/50, 1/30, and 1/15 radians of angle in the steel frame. At each displacement step, three cycles of load were applied by controlling displacement of the frame (DTP-500S transducer). Relative displacements between plate and each member were measured by displacement transducers (CDP-25 and CDP-50) for estimating rotational angles with corresponding applied moment (M). A perfect bilinear approximation was used to determine stiffness (R) and yielding moment (M_y). By contrast, this joint exhibited such

a high ductility that approximation was applied within 1/15 rad.

Results and discussion

Pull-out performance

Figure 12 and Table 3 show experimental results and calculated values for CW plate and doweled column–sill joints in pull-out tests. Yielding strength (P_y) of the joint with one dowel in the sill was 10.81 kN, and as the number of dowels increased, P_y increased in direct proportion to the number of dowels. Pull-out strength is thought to be controlled by the shearing strength of the dowel material at the sill. At the maximum strength (P_{max}) of the joint, the joint reached a load of 17.87 kN with one dowel. P_{max} increased with the number of dowels, but unlike P_y , it was not in direct proportion. This is due to the shift of failure mode from shearing in the wooden dowel for the one-dowel specimen to splitting or bending of the sill for two-dowel and three-dowel specimens. We conclude that the newly suggested mechanical model is quite acceptable even in this type of joint.

Rotational performance

The experimental results and values calculated by Table 4 are shown in Table 5 for joints with different numbers of dowels. Figure 13 shows curves of moment versus rotational angle response, and values calculated by the structural model for all kinds of joints. Coincidence was very good in each case. The yielding moment of the column was higher than that of the sill in each case. The yielding moment at the sill area was determined by shearing of dowel

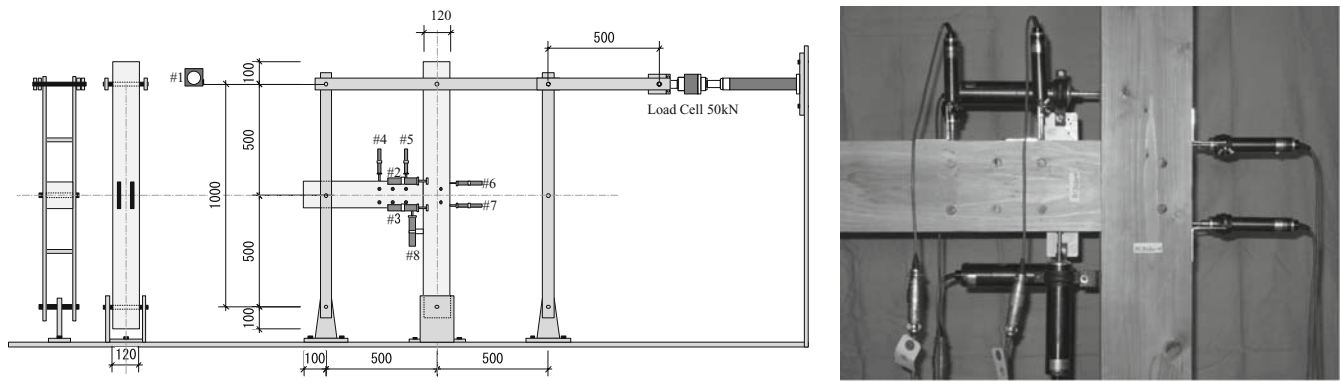


Fig. 11. Apparatus for rotation test of column-sill joint

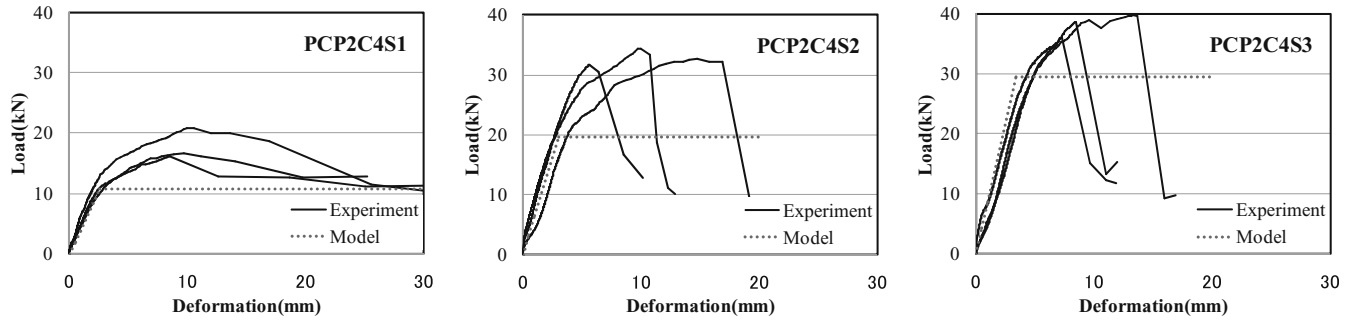


Fig. 12. Comparison between experimental and calculated values of deformation

Table 3. Results of pull-out tests on column-sill joint

Specimen	n_p	n_c	n_s	Calculated values		Experimental values			
				K_{model} (kN/mm)	$P_{y-model}$ (kN)	K_{exp} (kN/mm)	P_{y-exp} (kN)	P_{max} (kN)	E (kN.mm)
PCP2C4S1	2	4	1	3.91	9.82	4.47	10.81	17.87	190.27
PCP2C4S2	2	4	2	6.77	19.63	6.58	19.96	32.87	272.10
PCP2C4S3	2	4	3	8.95	29.45	6.36	27.61	38.14	253.04

K , Initial stiffness; P_y , yielding strength; P_{max} , maximum strength; E , energy

Table 4. Parameters for calculating by mechanical model

Double shear property of dowel								Compression property				μ	ρ (g/cm ³)
Stiffness (N/mm)				Yielding strength (N)				Stiffness (N/mm ²)		Yielding (N/mm ²)			
K_{b0p0d0}	$K_{b90p90d90}$	$K_{b90p0d0}$	$K_{b0p90d90}$	$P_{yb0p0d0}$	$P_{yb90p90d90}$	$P_{yb90p0d0}$	$P_{yb0p90d90}$	$E_{(CW90)}$	$E_{(Cedar90)}$	$E_{(Cedar0)}$	F_{m-CW}		
3145	3519	2216	3470	5296	4166	4581	5619	1000	240	6000	45	0.35	0.33

μ , Coefficient of friction; ρ , density

except for the no-dowel type in which embedding yield occurred.

Figure 14 shows values calculated by the structural model in comparison with the experimental envelope curve on the moment (M_j) of whole joint versus rotational angle (θ , θ_c , and θ_s) for each area. Stiffness of column area for two types showed no large difference. This is because the center two dowels are located close to rotation center. However, the

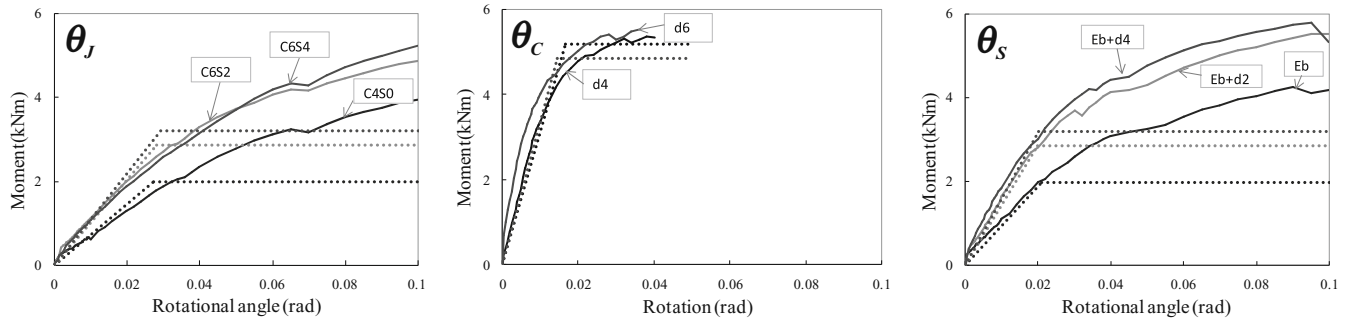
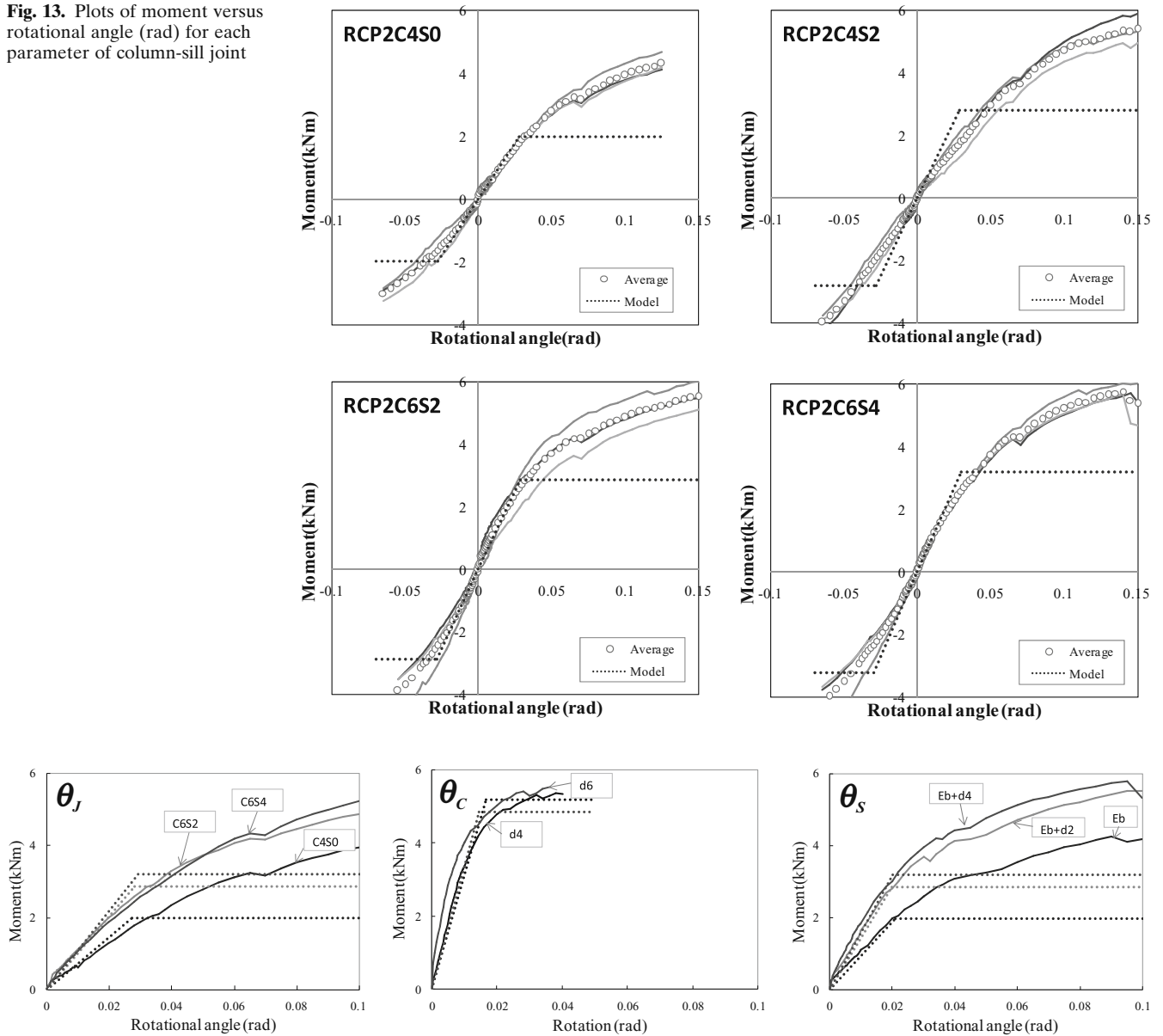
yielding moment for the six-dowel type was higher than that for the four-dowel type.

For the sill area, the effect of the number of dowels on stiffness was 1.5 times that of embedment when four dowels were inserted. Despite differences in stiffness between the two-dowel and four-dowel types being not very large, the yielding moment of the four-dowel type was higher than that of the two-dowel type. It is considered that the upper

Table 5. Comparison of calculated and experimental values

Specimen	Calculated values		Experimental values			
	R_{model} (kN.m/rad)	$M_{y\text{-model}}$ (kNm)	R_{exp} (kN.m/rad)	$M_{y\text{-exp}}$ (kNm)	M_{max} (kNm)	E (Nmrad)
PCP2C4S0	72.15	1.98	65.53	2.16	4.60	507.39
PCP2C4S2	97.31	2.79	70.74	2.64	5.78	715.50
PCP2C6S2	100.85	2.85	86.60	2.81	5.52	733.05
PCP2C6S4	108.69	3.20	93.13	2.76	5.78	721.43

R , Initial stiffness; M_y , yielding moment; M_{max} , maximum moment; E , energy

Fig. 13. Plots of moment versus rotational angle (rad) for each parameter of column-sill joint**Fig. 14.** Comparison between experimental and calculated values of moment on each area. *Left*, whole joint area; *middle*, column area; *right*, sill area

two dowels are located close to the rotation center of the sill area, so only the two bottom-side dowels were dominant in rotational stiffness. Although yielding of the sill area was determined by embedding, the yielding moment showed more improvement than stiffness with increasing dowel

number due to the rotational center (X_p) being shifted close to the center of gravity of the sill. Consequently, the embedding performance on the sill area by virtue of the CW strength is more dominant than shearing of dowel for rotational stiffness.

Conclusions

In this study, pull-out and rotational performance for a new type of column–sill joint were evaluated. The major conclusions are as follows:

1. For pull-out strength, the yielding strength was 10.81 kN and the maximum strength was 17.87 kN for the joint with one dowel inserted in the sill. The yielding strength increased linearly with the number of dowels at the sill, because this property was controlled by the dowel shear property.
2. For rotational performance, embedding performance on the sill area by virtue of the CW strength is more dominant than shearing of dowel for rotational stiffness. The effect of dowel on stiffness was 1.5 times that of embedding when four dowels were inserted.
3. In order to determine optimum joint design, a mechanical model was introduced by considering two deformation areas and two vector components separately. Theoretical performance was compared with experimental data. Consequently, this mechanical model was found to be valid.

Acknowledgments This research was carried out with support from the Japan Society for the Promotion of Science.

References

1. Jung K, Kitamori A, Leijten AJM, Komatsu K (2006) Effect of changes in moisture content due to surrounding relative humidity on contact stress in traditional mortise and tennon joints 3 (in Japanese). *Mokuzai Gakkaishi* 52:358–367
2. Nakata K, Komatsu K (2007) Development of timber portal frames compressed LVL plates and pins 1. *Mokuzai Gakkaishi* 53:313–319
3. Jung K, Kitamori A, Komatsu K (2008) Evaluation of structural performance of compressed wood as shear dowel. *Holzforschung* 62:461–467
4. Jung K, Kitamori A, Minami M, Komatsu K (2008) Development of joint system using compressed wooden fastener. *Proceedings of the 10th World Conference on Timber Engineering*, Miyazaki, Japan
5. Anonymous (2007) Allowable stress design method for timber housings. Japan Housing and Wood Technology Center, Tokyo, pp 56–58
6. Kitamori A, Jung K, Minami M, Komatsu K (2009) Evaluation on the stiffness of lattice shear wall (in Japanese). *J Struct Eng* 55B:109–116
7. Fukuyama H, Ando N, Inayama M, Takemura M, Inoue M (2007) Proposal of analytical models of wooden dowel shear joint. *J Struct Construct Eng* 622:129–136